materials

MDPI

Article

Study of Catalytic Combustion of Dioxins on Ce-V-Ti Catalysts Modified by Graphene Oxide in Simulating Iron Ore Sintering Flue Gas

Qi Shi [1], Long Ding [1], Hong-Ming Long [1,2,*] and Tie-Jun Chun [1]

[1] School of Metallurgical Engineering, Anhui University of Technology, Maanshan 243002, China; 13615556646@163.com (Q.S.); Dinglongahuter@163.com (L.D.); springcsu@126.com (T.-J.C.)

[2] Anhui Province Key Laboratory of Metallurgy Engineering & Resources Recycling; Anhui University of Technology, Maanshan 243002, China

* Correspondence: yaflhm@ahut.edu.cn

Received: 11 November 2019; Accepted: 24 December 2019; Published: 26 December 2019

Abstract: Ce-V-Ti and Ce-V-Ti/GO catalysts synthesized by the sol-gel method were used for the catalytic combustion of dioxins at a low temperature under simulating sintering flue gas in this paper. The catalytic mechanism of Ce-V-Ti catalysts modified with graphene oxides (GO) at a low temperature was revealed through X-ray diffractometer (XRD), Brunauer–Emmett–Teller (BET), transmission electron microscopy (TEM), X-ray photoelectron spectroscopy (XPS), H_2-temperature-programmed reduction (H_2-TPR) and Fourier transform infrared (FTIR). During the tests, chlorobenzene (CB) was used as a model reagent since the dioxins are poisonous. The results showed that introducing GO to Ce-V-Ti catalysts can improve the specific surface area and promote the CB adsorption on the surface of catalysts. Simultaneously, the Ce-V-Ti with 0.7 wt % GO support showed the high activity with the conversion of 60% at 100 °C and 80% at 150 °C. The adsorb ability of catalysts is strengthened by the electron interaction between GO and CB through π-π bond. In the case of Ce-V-Ti catalysts, Ce played a major catalytic role and V acted as a co-catalytic composition. After GO modification, the concentration of Ce^{3+} and V^{4+} were enlarged. The synergy between Ce^{3+} and V^{3+} played the critical role on the low-temperature performance of catalysts under sintering flue gas.

Keywords: iron ore sintering; dioxins emission; catalytic combustion; Ce/V/Ti catalysts; graphene oxide

1. Introduction

Dioxin (polychlorinated dibenzofurans and polychlorinated dibenzodioxins) can cause a series of environmental problems such as photochemical smog, atmospheric ozone depletion and ground-level ozone generation, which are considered to be extremely hazardous contaminants due to serious carcinogenicity and different discharges from the body [1]. It is mainly generated from a wide range of industrial processes or incineration of municipal and medical wastes. It is said that the iron ore sintering process is one of the largest emission sources [2]. Hence, the stringent environment regulations have been imposed on the emissions from the iron ore sintering process in many countries [3,4]. Among various control methods, catalytic combustion of dioxins at low temperature (100–200 °C) attracts considerable attention for energy conservation and emission reduction during the iron ore sintering process.

Catalysts are crucial for the catalytic combustion of dioxins at low temperature. During the past few decades there are a number of catalysts developed for dioxin catalytic combustion, most of which can be classified into three types: noble metals [5,6], transition metals [7,8] and zeolites [9,10]. Although the noble metal catalysts present excellent catalytic activity at high temperature, they are

susceptible to deactivation by chlorine adsorption. The activity of zeolites catalysts tends to fail gradually as the formation of polychlorinated compounds and the deposition of coke during catalytic combustion [11]. Recently, low-temperature catalytic combustion by transition metal oxides which can completely decompose these compounds has been considered as the most promising control technology owing to its low energy consumption, low cost, and good resistance to poisoning [12], especially for the effectively catalytic combustion at a low temperature from 200 °C to 400 °C without fuel combustion [13,14]. Nowadays, the catalytic combustion of dioxins has not been industrialized, so developing catalysts based on transition metal oxides with high catalytic activity at low temperature is of great significance.

It is reported that graphene oxide with oxygen functional groups is an excellent material for the functionalization of graphene and tunability of its optical properties due to its ultrathin two-dimensional (2D) sheets with 98% optical transmittance [15]. The graphene-based materials are promising for applications in supercapacitors and other energy storage devices due to highly tunable surface area, outstanding electrical conductivity, good chemical stability and excellent mechanical behavior [16].

In past research, V-Ti [17], Ce-Ti [11], V-Ce [18] and graphene-Ti [19] catalysts have been proved to have the ability of catalytic combustion of chlorobenzene (CB); However, introduced graphene oxide (GO) on the Ce-V-Ti catalysts to significantly improve the low temperature catalytic combustion of CB was never reported. In this work, a series of nanoparticles cerium vanadium titanium multi-metal oxide catalysts were prepared by the sol-gel method, and graphene oxide was introduced into Ce-V-Ti catalysts to pursue considerable catalytic conversion at low temperature under simulated sintering flue gas. In the presence of Ce-V-Ti/GO catalysts, the effect of modification on the chemical state of surface ions, oxygen vacancies and microstructure. Then, the catalytic mechanism was supposed on the results of characterizations.

2. Experimental and Material

2.1. Catalysts Preparation

Ce-V-Ti and Ce-V-Ti/GO catalysts were prepared by sol-gel method. Firstly, 3.78 g $Ce(NO_3)_3{\cdot}6H_2O$ ethanol solution was added to 34.10 g $Ti[O(CH_2)_3CH_3]_4$ ethanol solution under stirring. Then, 0.07 g commercial industrial graphene oxide (GO, purity > 97%, Chengdu Organic Chemicals Co. Ltd., Chengdu, China) with diameter of 3–10 μm was added without further treatment. The solution of NH_4VO_3 (0.64 g) and oxalic acid (n_{NH4VO3}:$n_{oxalic\ acid}$ = 1:1) was added under stirring. The solution was slowly gelled after finishing the reaction between $Ti[O(CH_2)_3CH_3]_4$ and H_2O at room temperature. The gel was dried at 110 °C for 12 h and then calcined at 450 °C for 3 h. The obtained samples were labeled as Ce-V-Ti and Ce-V-Ti/GO(x) catalysts, where x represented the weight percent of graphene oxide. TiO_2 was the carrier, CeO_2 was the active component, VO_X was the co-active component, and GO was the modified component in Ce-V-Ti/GO catalysts.

2.2. Catalyst Characterization

Characterization by XRD, BET, transmission electron microscope/high-resolution transmission electron microscopy (TEM/HRTEM), XPS, FTIR and H_2-TPR was carried out. The phase structures of catalysts were analyzed by a German D8ADVANCE X-ray diffractometer (XRD) with Cu K_α radiation (Cu K_α = 0.15406 nm, Brock, Germany). The surface area and distribution of pore size were carried out using an ASAP-2020 surface analyzer from Micromeritics, Norcross, GA, USA. Transmission electron microscopy (TEM) was performed with JEM-2100. X-ray photoelectron spectroscopy (XPS) was used to analyze the oxidation states on the surface of the CeO_2-VO_x-TiO_2/GO catalysts with AXIS ULTRP, which used Al Kα (1486.6 eV) radiation as the excitation source (powered at 10 mA and 15 kV). The temperature-programmed reduction (H_2-TPR) test was carried out by an N-3000 dual-channel chromatography workstation device. FT-IR spectra were recorded at room temperature

on a Fourier Transform Infrared Spectrometer (5DXC, Nicolet6700, Nicolet, Glendale, WI, USA) in the 500–4000 cm^{-1} range and a resolution of 4 cm^{-1}.

2.3. Apparatus and Methods

Catalytic conversion was tested in a fixed-bed flow reactor as shown in Figure 1, in which 200 mg (grain size, 40–60 mesh) catalysts were placed in a silica tube with 3 mm inner diameter. Due to the complex structure, strong toxicity and troublesome analysis of dioxins, chlorobenzene (CB) was generally used as a model reagent in laboratories [20,21]. The total flow rate through the reactor was set at 100 standard-state cubic centimeter per minute (S ccm), corresponding to a gas hour space velocity (GHSV) 30,000 h^{-1}. Feed stream to the reactor was prepared by delivering liquid CB with a syringe pump, and the injection position was cooled with ice water bath to ensure the complete evaporation of the liquid reactor feeds. The reaction flue gas was composed of 16% O_2 and 84% N_2, and the CB concentration was set to 100 ppm to simulate iron ore sintering flue gas. The reaction temperature was controlled with a thermocouple. The recent gases were analyzed under a given temperature by using an online gas chromatograph (GC) equipped with flame ionization detector (FID1) and SE-54 capillary column for the quantitative analysis the inlet and outlet of CB. During the CB analysis the temperature of the column and detector of GC with nitrogen as carrier gas were set up as 100 °C and 150 °C, respectively.

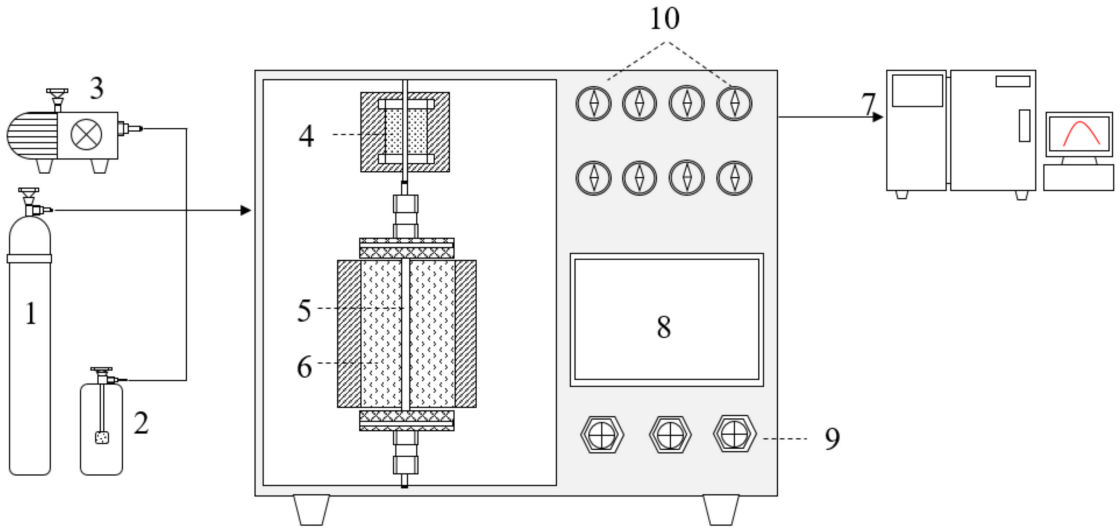

Figure 1. Chlorobenzene (CB) oxidation reaction device. 1 gas cylinder; 2 CB generator; 3 air pumps; 4 preheating furnaces; 5 silica tube; 6 holding furnace; 7 gas chromatograph (GC); 8 controlling panel; 9 controlling valve; 10 pressure gages.

The conversion ratio of CB (η) was calculated as follows:

$$\eta = \frac{CB_{in} - CB_{out}}{CB_{in}} \times 100\%$$

where the CB_{in} and CB_{out} were the inlet and outlet concentration of CB in the system at steady-state, respectively.

3. Results and Discussion

3.1. Catalytic Activity Analysis

The catalytic activity of CB over Ce-V-Ti and Ce-V-Ti/GO catalysts is shown in Figure 2. The Ce-V-Ti catalysts showed good activity with a 90% conversion at 300 °C. After modification by GO, the activity

of the catalysts increased significantly and showed high catalytic activity between 100–250 °C. The Ce-V-Ti/GO(0.7) catalysts achieved 90% conversion at 200 °C, which is 100 °C lower than Ce-V-Ti catalysts.

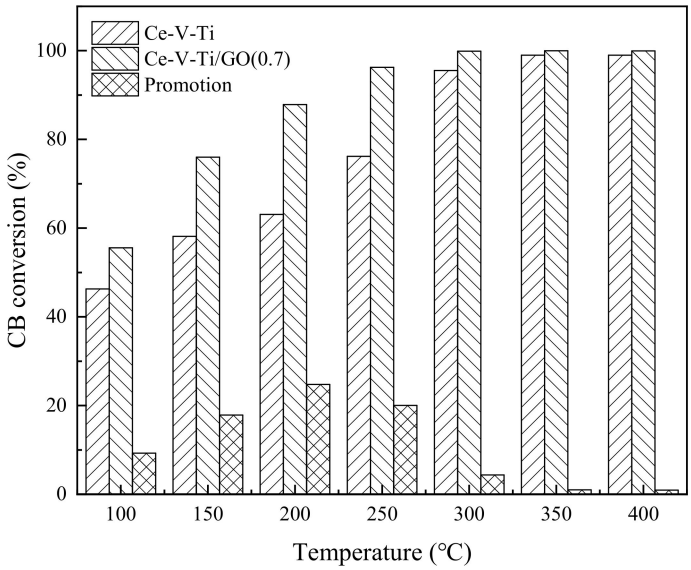

Figure 2. CB conversion over Ce-V-Ti and Ce-V-Ti/GO catalysts; CB: 100 ppm; gas hour space velocity (GHSV): 30,000 h^{-1}; catalyst amount: 200 mg.

Research about catalytic combustion of dioxins over metal oxide catalysts is shown in Table 1. It can be seen that normal transition metal oxides catalysts showed low CB conversion at 150 °C and T_{90} are all above 225 °C. The catalytic activity at low temperature over Ce-V-Ti/GO catalysts was observably higher than those catalysts. Ce-V-Ti/GO catalysts can achieve near 60% CB conversion at 100 °C and 75% CB conversion at 150 °C, which was more suitable for catalytic combustion of dioxins from the sintering process with relatively low temperature after desulfurization (the temperature of sintering flue gas after desulfurization is about 100–150 °C).

Table 1. Research about the catalytic combustion of CBs over metal oxide catalysts.

Samples	$C_{150\,°C}$	T_{90}	Reaction Condition	Ref.
$Ce_{0.5}Ti_{0.5}$	0%	375 °C	1000 ppm CB; 10% O_2/N_2; GHSV = 30,000 h^{-1}	[22]
$Cr_{0.75}Ce_{0.25}/Ti$	20%	225 °C	500 ppm CB; GHSV = 20,000 h^{-1}	[23]
$Mn_6Co_2Ce_2$	20%	325 °C	500 ppm CB; GHSV = 15,000 h^{-1}	[24]
Ru (1%)/TiO_2-CeO_2	5%	225 °C	550 ppm CB; GHSV = 15,000 h^{-1}	[25]
VO_x (2.1%)/CeO_2	5%	225 °C	1000 ppm CB; GHSV = 30,000 h^{-1}	[26]
$Cu_{0.15}Mn_{0.15}Ce_{0.7}O_x$	2%	255 °C	600 ppm CB; 21%$O_/N_2$; GHSV = 30,000 h^{-1}	[27]
Mn (0.86)-CeLa	20%	250 °C	1000 ppm CB; 10%$O_/N_2$; GHSV = 15,000 h^{-1}	[28]
MnO_X (0.86)-CeO_2	20%	236 °C	1000 ppm CB; 10%$O_/N_2$; GHSV = 15,000 h^{-1}	[29]

$C_{150\,°C}$: the catalytic activity at 150 °C; T_{90}: the temperature of 90% CB conversion.

For industrial applications, the stability in catalytic activity is essential for long-time operation. Figure 3 was the stability test of catalysts at 200 °C. The Ce-V-Ti/GO and Ce-V-Ti/GO(0.7) catalysts showed stable activity after 200 min and kept steady CB conversion within 1000 min. The CB conversion over Ce-V-Ti/GO and Ce-V-Ti/GO(0.7) catalysts were about 50% and 75%, respectively. Compared with the activity of fresh Ce-V-Ti/GO catalysts (Figure 2), it can be seen that the activity drops at 200 min. The deactivation is related to the strong adsorption of HCl or Cl_2 produced during catalytic reaction [8]. In order to further confirm the deactivation of the catalyst was due to chloride poisoning, XPS was used to detect the Cl ions on the surface of the deactivated catalyst, as shown in the right

corner of Figure 3. It showed that on the surface of the deactivated catalyst appeared Cl ion spectral peak located at 198.6 eV, while it cannot be detected on the surface of the fresh catalyst. The results showed that Ce-V-Ti catalysts were partially deactivated in the catalytic reaction by chlorine poisoning. The catalytic activity of Ce-V-Ti/GO and Ce-V-Ti/GO(0.7) catalysts recovered partly and kept stable as the catalytic reaction went on. CO/CO_2 in off-gas were analyzed by online gas chromatograph (GC) equipped with a flame ionization detector (FID). Because of the sufficient oxygen in the reaction gas, no CO was detected. It indicated that CB was complete combustion during the Ce-V-Ti and Ce-V-Ti/GO catalysts combustion reaction. HCl/Cl_2 were detected by ion chromatography (LC-2010 PLUS) after adsorption by NaOH solution. The result was analyzed strongly with HCl and Cl_2 in Figure 4. The collected Cl species were the product of the reductive dichlorination of CB. The removal of Cl^- and H^+ can combine to produce HCl, and Cl_2 is attributed to Deacon Reaction ($2HCl + 1/2O_2 \rightarrow Cl_2 + H_2O$), which inevitably generates Cl_2. These indicated that CB underwent a completely catalytic oxidation into CO_2, H_2O and HCl/Cl_2 by the detection of CO_2 and Cl species.

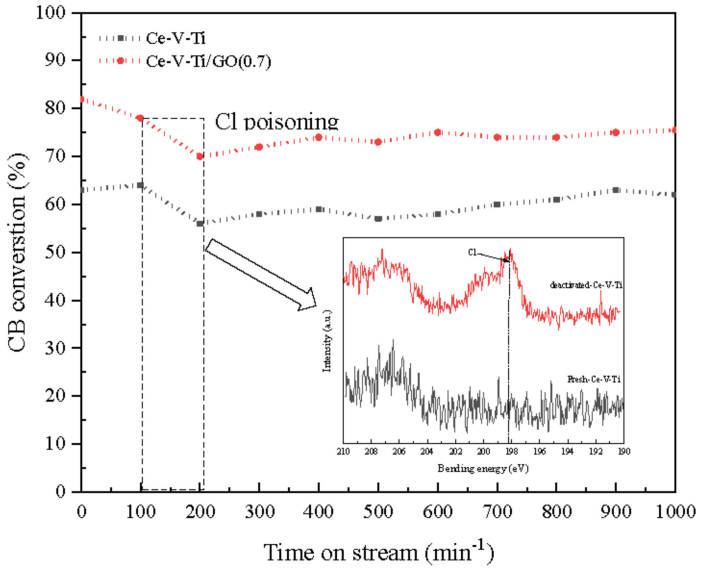

Figure 3. Stability for the CB catalytic combustion over Ce-V-Ti/GO at 200 °C. CB concentration: 100 ppm; GHSV: 30,000 h^{-1}; catalyst amount: 200 mg.

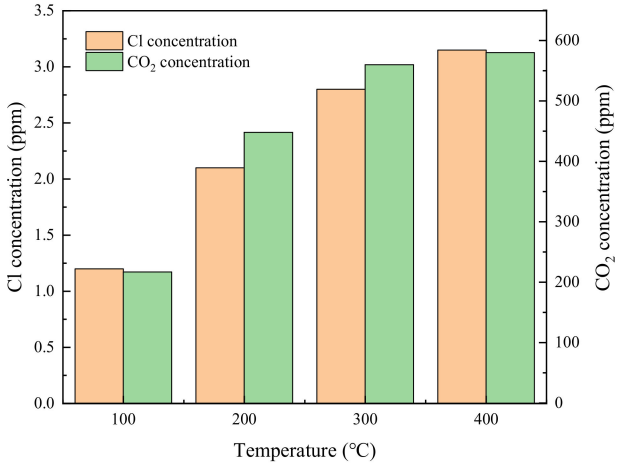

Figure 4. Main products of CB combustion over Ce-V/Ti-GO(0.7) catalysts. CB concentration: 100 ppm; GHSV: 30,000 h^{-1}; catalyst amount: 200 mg.

3.2. Textural Properties

The N_2 adsorption-desorption isotherms revealed the textural properties of the samples. The BET surface area, pore volume, and pore size of the Ce-V-Ti and Ce-V-Ti/GO catalysts are summarized in Table 2. The specific surface area of the Ce-V/Ti catalyst was 95.7 m^2/g and increased to 123.8 m^2/g after adding GO. Meanwhile, the pore volume decreased from 0.29 to 0.15 cm^3/g after adding GO, and the pore diameter remained nearly similar. The results indicated that Ce-V-Ti/GO catalysts had porous structures. Studies [30,31] have shown that a high volume of mesopores was available for the dispersion of metal oxide particles. After modification by GO, the specific area and pore volume was optimized, which was consistent with the TEM photographs. In general, large specific surface areas and porous structures are expected to improve the catalytic performance by providing more active sites, which favored the adsorption of reactants. It can account for the excellent catalytic performance of Ce-V-Ti/GO catalysts.

Table 2. Textural properties of the catalysts.

Sample	Surface Area (m^2/g) [a]	Total Pore (cm^3/g) [b]	Average Pore (nm) [c]
Ce-V-Ti/GO(0.7)	123.8	0.15	6.4
Ce-V-Ti	95.7	0.29	6.5

[a] Determined by BET surface area. [b] Adsorbed volume at $P/P_0 = 0.995$. [c] Determined by desorption branch.

XRD characterization was performed to study the internal crystal structure of the samples (Figure 5). All samples showed the characteristic peaks of anatase TiO_2 in the in 10–80° range (25.3, 37.8, 48.1, 53.9, 55.1, 62.6, 68.7, 70.3, 74.9, and 84.6°; JCPDF # 21-1272) [32]. No obvious diffraction peaks ascribed to the crystalline cerium oxides or vanadium oxides were observed in the Ce-V-Ti catalysts, which indicated that Ce-V mixed oxides might have low crystallinity. The diffraction pattern of the Ce-V-Ti/GO catalysts contained peaks at 28.6, 33.0, 56.3, 59.0, and 76.6°, and was indexed to the face-centered cubic phase of CeO_2 (JCPDF # 43-1002) [19]. These results indicated that the addition of GO could have promoted the crystallization of CeO_2 by hindering the forming of a Ce-O-Ti solid solution. No diffraction peaks characteristic of carbon species was observed owing to the low carbon loading and the relatively low diffraction intensity of GO. Thus, the presence of GO was further determined by XPS.

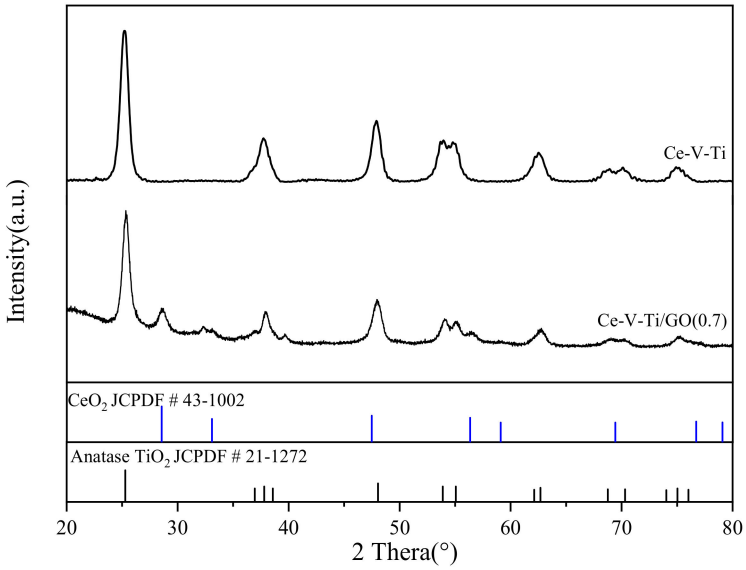

Figure 5. X-ray diffractometer (XRD) patterns of the Ce-V-Ti and Ce-V-Ti/GO catalysts.

The morphology of the catalysts was characterized by TEM. As shown in Figure 6a–d, the microstructures of Ce-V-Ti and Ce-V-Ti/GO(0.7) catalysts were nanoparticles. Small CeO_2 particles were found on the Ti-based structures. The lattice spacing (0.312 nm) matched that of the <111> crystal plane of a standard CeO_2 sample (JCPDF #43-1002). Along with CeO_2 particles, the TiO_2 particles showed an exposed <101> crystal plane with a lattice spacing of 0.352 nm (anatase, JCPDF #21-1272).

Figure 6a shows TEM images of Ce-V-Ti catalysts without GO modification. These catalysts showed serious grain aggregation on the surface, which could explain the low CB conversion of catalysts. After GO modification, the Ce-V-Ti catalysts were found to contain dispersed nanoparticles on the flaky GO (Figure 6c,d). Figure 6c reveals large areas of transparent and flaky GO with many folds, and Ce-V-Ti nanoparticles were uniformly and highly dispersed on this material. The Ce-V-Ti/GO(0.7) catalysts were highly efficient in the catalytic combustion of CB at low temperature.

The TEM images also showed that the catalysts were homogeneous with no crystalline vanadium oxide phases. To further characterize the distribution of vanadium species in the catalysts, elemental mapping was conducted on Ce-V-Ti/GO(0.7) by scanning electron microscopy (SEM). As shown in Figure 7, the vanadium species were uniformly and highly dispersed on TiO_2 in Ce-V-Ti/GO(0.7) catalysts.

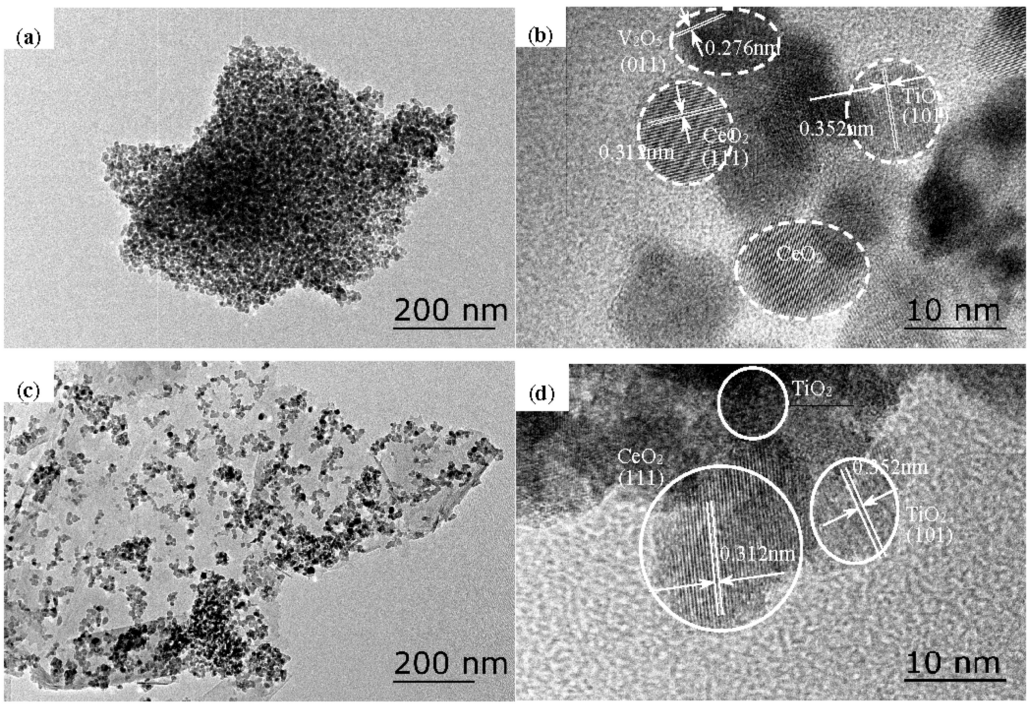

Figure 6. Transmission electron microscropy (TEM) images of catalysts: (**a**,**b**) Ce-V-Ti, (**c**,**d**) Ce-V-Ti/GO(0.7).

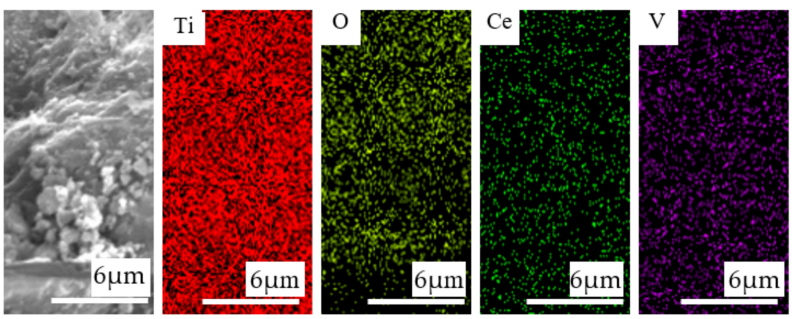

Figure 7. Scanning electron microscopy (SEM) images and mapping images of the Ce-V-Ti/GO(0.7) catalysts.

3.3. Surface Properties

The atomic concentration and element chemical state on the catalyst surface was investigated by XPS. Figure 8a–c shows the Ce 3d, O 1s, and V 2p XPS spectra, respectively. The corresponding surface atomic concentrations and the relative concentration ratio of the different oxidation states are summarized in Table 3. As shown in Figure 8a, the Ce 3d orbit contained two multiples (v and u). The u, u″, u‴, v, v″ and v‴ peaks were attributed to Ce^{4+} species, while u′ and v′ were assigned to Ce^{3+} species [33,34]. There were some changes in the intensity and position of the Ce 3d bands between Ce-V-Ti and Ce-V-Ti/GO catalysts. As indicated in Table 3, Ce-V-Ti/GO(0.7) showed a significantly higher amount of surface Ce^{3+} species than the rest of the catalysts.

The fraction of Ce^{3+} ions can be stabilized by decreasing the energy of the Ce 4f levels. The reducibility of ceria was not infected by the fraction Ce^{3+} ions that were already present. As the additional electrons in Ce^{3+} occupy localized cerium 4f- states, Ce^{3+} ions did not interact with the reducibility of catalysts [4]. These Ce^{3+} species could create vacancies with one-charge imbalances and unsaturated chemical bonds on the catalyst surface, which could increase the amount of surface chemisorbed oxygen [34]. After adding 0.7% of GO, the amount of reduced Ce^{3+} ions increased. It indicated that GO changed the chemical environment and the oxidation state of Ce [35].

The O 1s spectra (Figure 8b) were deconvoluted into two contributions: one at a binding energy (BE) of 529.3–529.8 eV were assigned to lattice oxygen (O_β) and the other BE at 531.0-531.4 eV were assigned to surface-adsorbed oxygen species (O_α) such as O_2^{2-} or O^- [36]. The peak shifts between Ce-V-Ti and Ce-V-Ti/GO revealed that the interaction between Ce-O-Ti can changed the structure and electron configurations. In the presence of GO, the BE of O_α shifted to lower values due to "Ce←O" electron-transfer processes through the formation of Ce-O-Ti. Moreover, the amount of O_α (estimated by peak area) increased with the amount of Ce species (Table 3). Thus, Ce species were mostly responsible for the onset of O_α. The Ce-V-Ti/GO(0.7) catalysts showed the highest concentration of Ce^{3+} and a considerable amount of active surface oxygen chemically adsorbed on the vacancies (O^-). Thus, Ce-V-Ti/GO(0.7) showed the highest activity for the catalytic combustion of CB.

Table 3. Atomic surface compositions of Ce-V-Ti and Ce-V-Ti/GO catalysts obtained by X-ray photoelectron spectroscopy (XPS).

Sample	Atomic (%)							
	Ce	V	O	C	Ce		O	
					Ce^{3+}	Ce^{4+}	O_α	O_β
Ce-V-Ti	5.56	0.91	63.44		20	80	88	12
Ce-V-Ti/GO(0.7)	6.96	1.01	65.82	1.66	30	70	53	47

Figure 8c shows XPS curves of surface vanadium species. No obvious difference was observed in the V 2p spectra. In all samples, the V $2p_{3/2}$ level at about 516 eV was ascribed to V^{4+} species [37]. As reported previously, oxidized vanadium was stable when deposited on titanium [32], cerium, or reduced cerium [38]. Higher amounts of V^{4+} (within a certain value) increased the amount of Lewis acid on the surface [37]. V^{4+} was oxidizable and can assist in the reduction of Ce^{4+} to accelerate the reaction catalytic cycle.

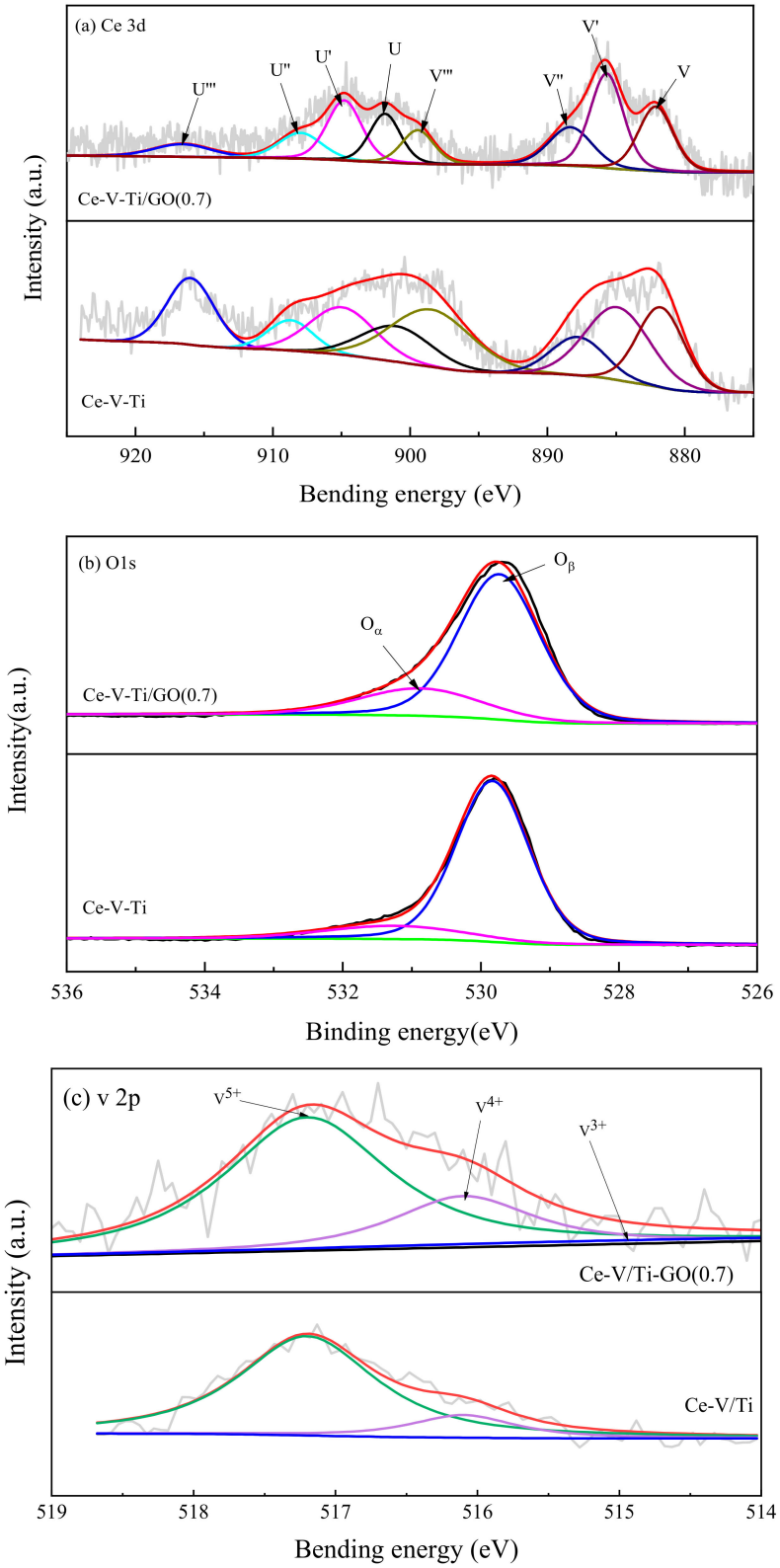

Figure 8. XPS spectra for: Ce 3d (**a**), O 1s (**b**), and V 2p (**c**) of the catalysts.

3.4. FTIR Spectra and H_2-TPR Analysis

The samples were analyzed by FTIR to study the effects of GO doping on Ce-V-Ti catalysts (Figure 9). The absorption bands from 3200 to 3700 cm^{-1} were attributed to O-H stretching vibrations of hydroxyl, carboxylic, and phenolic groups [39]. The adsorption bands at 1610–1680 cm^{-1} could be

attributed to C=C stretching vibrations in carboxylic or pyridine-like structures [40]. The bands at 2700–3000 and 1360–1480 cm^{-1} could be attributed to the stretching and vibration bending vibrations of aliphatic C-H groups, respectively [41]. The bands at 1050–1160 cm^{-1} were ascribed to the bending vibrations of C-O groups [18]. Figure 9 shows that surface functional groups of O-H (3417 cm^{-1}), C-H (1388, 1455, 2923, and 2952 cm^{-1}), C=O (1064 cm^{-1}), and C=C (1631 cm^{-1}) existed in Ce-V-Ti and Ce-V-Ti/GO catalysts.

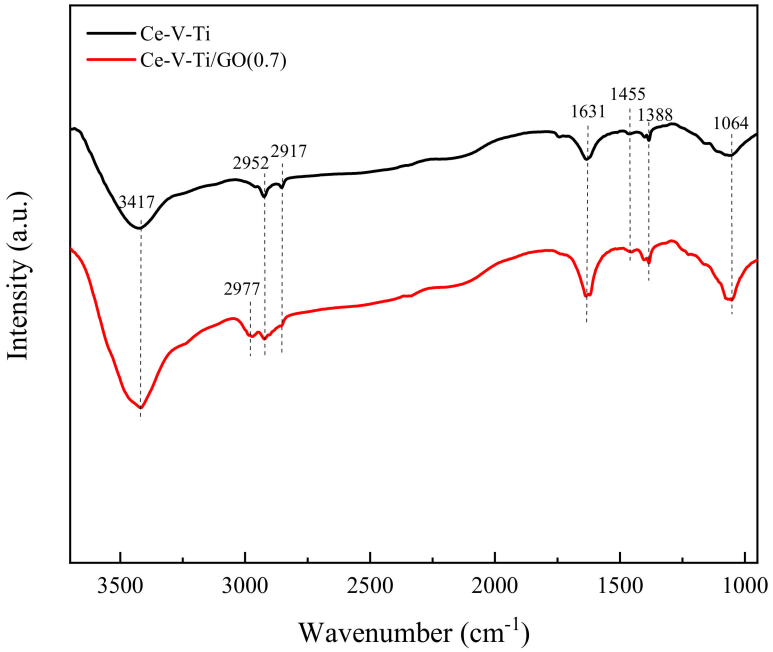

Figure 9. Fourier transform infrared (FTIR) spectra of the Ce-V-Ti and Ce-V-Ti/GO catalysts.

The 3417 cm^{-1} peaks were more intense in the Ce-V-Ti/GO catalysts than in the GO-free catalysts. Ce-V-Ti/GO(0.7) catalysts showed a new peak at 2917 cm^{-1}. The peaks at 2917 and 3417 cm^{-1} were attributed to aliphatic C-H groups and O-H stretching vibrations in hydroxyl, carboxylic, and phenolic groups, respectively. Hence, the addition of GO strengthened the intensity of aliphatic C-H groups and O-H stretching vibrations, increased the number of hydroxyls, carboxylic, and phenolic acids and favored new aliphatic C-H groups (2917 cm^{-1}). As a consequence, these groups favored the adsorption of CB on Ce-V-Ti/GO catalysts, facilitating the desorption of CB [42].

H_2-TPR was used to investigate the reducibility of surface oxygen on Ce-V-Ti and Ce-V-Ti/GO catalysts within 200–700 °C (Figure 10). The H_2-TPR plots of Ce-V-Ti catalysts mainly exhibited a two-step reduction peak of surface ceria and vanadium oxides. The reduction peak centered at ca. 460 °C might be ascribed to the reduction of VOx species [43]. The peak at higher temperatures (370–594 °C) was ascribed to the reduction of high valent ceria ions (from CeO_4 to Ce_2O_3) [44]. After the addition of GO, the reduction peak of vanadium at 459 °C gradually overlapped with the reduction peak of cerium. The reduction peak of ceria slightly shifted to lower temperatures (shoulder at 565 °C–560 °C from Ce-V-Ti to Ce-V-Ti/GO catalysts). Meanwhile, the consumption of H_2 was increased with GO addition. Further reduction reaction was facilitated with the increasing temperature, which resulted in a higher number of Ce^{3+} ions [18]. Interestingly, the reduction of Ce^{4+} to Ce^{3+} on the surface of nano-crystallites with different sizes was observed in the H_2-TPR plots of Ce-V-Ti/GO(0.7) [45]. It indicated that the reduction of Ce^{4+} was promoted after adding GO [11]. The interaction between Ce and Ti increased the number of surface defects and active oxygen, thereby facilitating the reduction temperatures (reduction peaks of the Ce-V-Ti and Ce-V-Ti/GO were 357 and 348 °C, respectively). Therefore, the low temperature activity of CB over Ce-V-Ti catalysts with appropriate GO modification were improved by promoting the reduction of the active components.

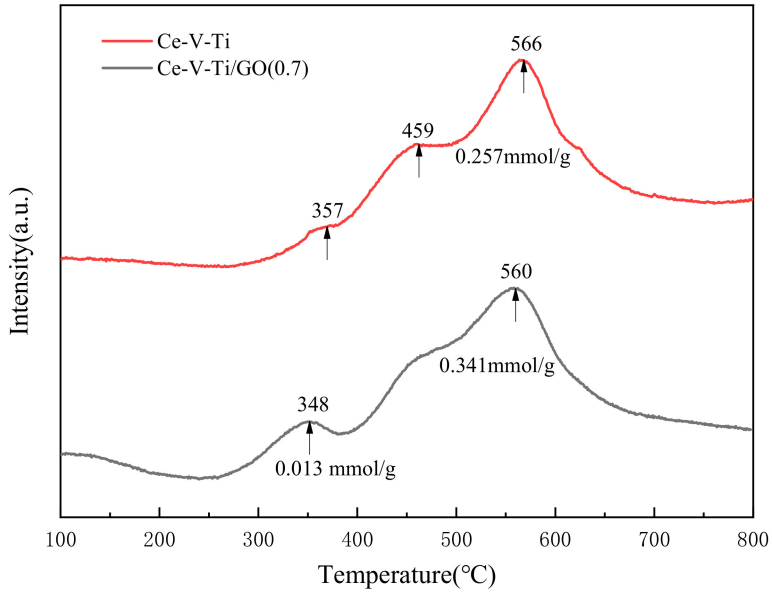

Figure 10. Temperature-programmed reduction (H_2-TPR) profiles of the Ce-V-Ti and Ce-V-Ti/GO catalysts.

3.5. Proposed Reaction Mechanism Analysis

The catalytic activity test showed that CB combustion over Ce-V-Ti catalysts was higher than most normal catalysts at low temperature. It was because the nano-TiO_2 content of Ce-V-Ti catalysts efficiently increased the specific surface area, which could result in a high distortion extent. After being modified by GO, the low temperature catalytic activity of Ce-V-Ti catalysts was further improved.

Generally, CB combustion over the Ce-V-Ti catalyst was the Deacon reaction and followed the MVK mechanism [14]. The chlorine of CB released during catalytic combustion was adsorbed on the metal active sites (Ce^{3+}/Ce^{4+} and V^{3+}). Chlorine was adsorbed by nucleophilic oxygen (basic lattice oxide ions or hydroxyl groups) to form a phenolate intermediate. The catalysts adsorbed the gas-phase oxygen on the active sites to replenish the consumed oxygen. The active surface oxygen species attacked the aromatic ring, and finally oxidized CB into CO_2 and H_2O. To obtain deeper insight into this reaction at the molecular level, the mechanism of CB combustion over Ce-V-Ti catalysts was proposed based on the above analyses.

First, the oxidation and reduction reactions could proceed between CeO_2 and VO_x. Here, O* includes O_2^-, O^-, and O^{2-}.

$$CeO_2 \rightarrow Ce_2O_3 + O^*$$

V acted as a co-catalyst in the CeO_2/VO_x catalysts. During the oxidation process, oxygen could transfer from Ce-OH to VO_x. It may promote the rate of cyclic catalytic reactions by accelerating electron transfer between Ce and V. The presence of V^{3+} improved the catalytic activity and ensured faster electron transfer during the mutual transformation of V^{3+} and Ce^{4+}.

$$VO_x + Ce^{4+} + O^{2-} \rightarrow V_2O_5 + Ce^{3+}$$

In the third step, according to the MVK mechanism, O* attacked CB and oxidized CB into HCl, CO_2, and H_2O on the active sites of the catalyst. The CB molecules were then adsorbed on the surface of the catalysts. The C-Cl molecular bond of CB break on the surface of the catalyst and degraded into an intermediate, which in turn degraded into CO_2 and H_2O and simultaneously produced HCl.

$$C_6H_5Cl + O \rightarrow HCl + CO_2 + H_2O$$

Fourth, Ce_2O_3 captured O from oxygen on the surface of the catalysts and was re-oxidized to CeO_2.

$$Ce^{3+} + \frac{1}{4}O_2 \rightarrow Ce^{4+} + \frac{1}{2}O^{2-}$$

Hence, catalytic combustion was a process of catalytic combustion and adsorption. Improving the rate of catalytic combustion and the adsorption capacity of the catalyst could effectively improve catalytic activity. Consequently, adding GO into Ce-V-Ti catalysts can increase catalytic activity by enhancing adsorb ability and changing the adsorption mode. GO possessed a similar layered structure to graphene, and was heavily decorated with oxygen-containing groups on the planes or carbon atoms [15]. Studies have shown that the removal efficiency of dioxins, of which long axis was 1.4 nm, short axis was 0.74 nm, and the thickness was 0.35 nm [46], was related to the specific surface area and the medium pore volume of carbon materials [47]. The specific surface area was larger and the medium pore size was closer to the dioxin molecule size in Ce-V-Ti/GO catalysts after adding GO (diameter is 3–10 μm, S_{BET} is 500–1000 m^2/g). It was consistent with the catalytic activity of Ce-V-Ti/GO catalysts.

After adding GO, the adsorption mode could be changed from vertical adsorption mode to parallel adsorption mode, as shown in Figure 11. The CB molecule was vertically adsorbed to the surface of Ce-V-Ti catalysts by nucleophilic substitution (C-Cl bond breaking). It was reported that aromatic organic compounds can be adsorbed to the surface of GO through the force of π-π bond [48]. The results of FTIR show that carboxyl (-COOH) was increased with introduced GO into Ce-V-Ti catalysts. Carboxyl groups can provide electronic for π-π bonds, while CB gets electronic from π-π bonds. Consequently, the adsorption ability was enhanced by adding GO with the electron interaction. Besides, the results of XPS show that small amounts of GO can promote the amount of Ce on the surface, especially the amount of Ce^{3+} ions. The chemical interaction between Ce and Ti could improve the amount of oxygen vacancies and Ce^{3+} ions, both of which can effectively improve the adsorption of acidic sites on the catalysts surface. In addition, a certain amount of low-priced vanadium oxides appeared in Ce-V-Ti/GO catalysts, which could help promote the rate of catalytic combustion through accelerating the recycle reaction of Ce.

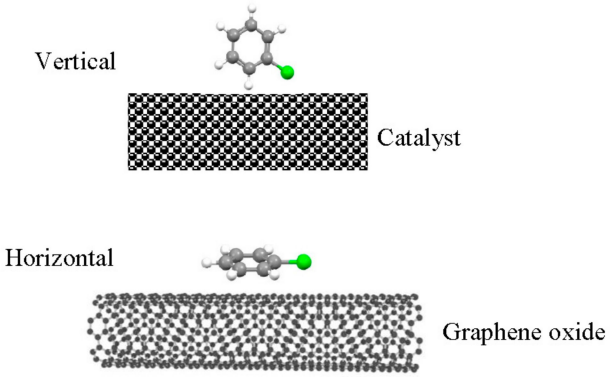

Figure 11. The adsorption model on the catalyst surface.

4. Conclusions

(1) The catalytic activity of Ce-V-Ti catalysts was improved significantly after modification with GO. The CB conversion over Ce-V-Ti/GO catalysts achieved 60% at 100 °C and 80% at 150 °C, which showed excellent catalytic activity at low temperature.

(2) After being modified with GO, the specific surface area and adsorb ability of CB were both enhanced. The concentration of Ce^{3+} and V^{4+} on the surface was enlarged, which corresponded with oxygen vacancies. Moreover, the adsorption mode could be changed from a vertical adsorption mode to a parallel adsorption mode by interaction of π-π bonds between CB and GO.

(3) Ce played a major catalytic role and V acted as a co-catalytic composition during catalytic combustion. The chemical interaction between Ce and Ti could improve the amount of oxygen vacancies and Ce^{3+} ions. V^{3+} could help to promote the reduction reaction.

Author Contributions: Q.S. designed the study. Q.S. and L.D. completed the preparation of catalysts; H.-M.L. designed the catalytic combustion tests. Q.S., T.-J.C. and L.D. contributed to sample preparation and material characterization. H.-M.L. and T.-J.C. supervised the research. All authors discussed the results and contributed the final manuscript. All authors have read and agreed to the published version of the manuscript.

Funding: The authors acknowledge financial support from General Program of National Nature Science Foundation of China (51674002) and the Key Project of National Nature Science Foundation of China (U1660206).

Conflicts of Interest: The authors declare no conflict of interest.

References

1. Sun, P.; Wang, W.; Dai, X.; Weng, X.; Wu, Z. Mechanism study on catalytic oxidation of chlorobenzene over $Mn_XCe_{1-X}O_2$/H-ZSM5 catalysts under dry and humid conditions. *Appl. Catal. B Environ.* **2016**, *198*, 389–397. [CrossRef]
2. Qian, L.; Chun, T.; Long, H.; Li, J.; Di, Z. Emission reduction research and development of PCDD/Fs in the iron ore sintering. *Process Saf. Environ.* **2018**, *117*, 82–91. [CrossRef]
3. Wang, C.; Zhang, C.; Hua, W.; Guo, Y.; Lu, G.; Gil, S.; Giroir-Fendler, A. Catalytic oxidation of vinyl chloride emissions over Co-Ce composite oxide catalysts. *Chem. Eng. J.* **2017**, *315*, 392–402. [CrossRef]
4. Yang, S.; Zhao, H.; Dong, F.; Zha, F.; Tang, Z. Highly efficient catalytic combustion of o-dichlorobenzene over three-dimensional ordered mesoporous cerium manganese bimetallic oxides: A new concept of chlorine removal mechanism. *Mol. Catal.* **2019**, *463*, 119–129. [CrossRef]
5. Aristizábal, B.H.; Maya, C.; Correa, C.M.D. Ortho-dichlorobenzene oxidation over Pd/Co loaded sulfated zirconia and mordenite catalysts. *Appl. Catal. A Gen.* **2008**, *335*, 211–219. [CrossRef]
6. Ma, X.; Shen, J.; Pu, W.; Sun, H.; Pang, Q.; Ma, X. Water-resistant Fe-Ca-O_x/TiO_2 catalysts for low temperature 1,2-dichlorobenzene oxidation. *Appl. Catal. A Gen.* **2013**, *466*, 68–76. [CrossRef]
7. Amorós-Pérez, A.; Cano-Casanova, L.; Castillo-Deltell, A.; Lillo-Ródenas, Á.M.; Román-Martínez, C.M. TiO_2 Modification with Transition Metallic Species (Cr, Co, Ni, and Cu) for Photocatalytic Abatement of Acetic Acid in Liquid Phase and Propene in Gas Phase. *Materials* **2019**, *12*, 40. [CrossRef]
8. Lu, S.; Wang, Q.; Stevens, W.R.; Lee, C.W.; Gullett, B.K.; Zhao, Y. Study on the decomposition of trace benzene over V_2O_5-WO_3/TiO_2-based catalysts in simulated flue gas. *Appl. Catal. B Environ.* **2014**, *147*, 322–329. [CrossRef]
9. Gutiérrez-Ortiz, J.I.; López-Fonseca, R.; Aurrekoetxea, U.; González-Velasco, J.R. Low-temperature deep oxidation of dichloromethane and trichloroethylene by H-ZSM-5-supported manganese oxide catalysts. *J. Catal.* **2003**, *218*, 148–154. [CrossRef]
10. López-Fonseca, R.; de Rivas, B.; Gutiérrez-Ortiz, J.I.; González-Velasco, J.R. Enhanced activity of zeolites by chemical dealumination for chlorinated VOC abatement. *Appl. Catal. B Environ.* **2003**, *41*, 31–42. [CrossRef]
11. Deng, W.; Dai, Q.; Lao, Y.; Shi, B.; Wang, X. Low temperature catalytic combustion of 1,2-dichlorobenzene over CeO_2-TiO_2 mixed oxide catalysts. *Appl. Catal. B Environ.* **2016**, *181*, 848–861. [CrossRef]
12. He, F.; Luo, J.Q.; Liu, S. Novel metal loaded KIT-6 catalysts and their applications in the catalytic combustion of chlorobenzene. *Chem. Eng. J.* **2016**, *294*, 362–370. [CrossRef]
13. Dai, Q.; Wang, X.; Lu, G. Low-temperature catalytic combustion of trichloroethylene over cerium oxide and catalyst deactivation. *Catal. Commun.* **2008**, *3*, 192–202. [CrossRef]
14. Dai, Y.; Wang, X.; Dai, Q.; Li, D. Effect of Ce and La on the structure and activity of MnO_x catalyst in catalytic combustion of chlorobenzene. *Appl. Catal. B Environ.* **2012**, *111*, 141–149. [CrossRef]
15. Pei, S.; Cheng, H. The reduction of graphene oxide. *Carbon* **2012**, *50*, 3210–3228. [CrossRef]
16. Samia, A.; Faiza, M.; Muhammad, A.A. Facile synthesis of graphene oxide with significant enhanced properties for optoelectronic and energy devices. *Ceram. Int.* **2018**, *44*, 6823–6828.
17. Chiraz, G.; Romain, D.; Pierre, E.; Damien, P.D.; Abdelhamid, G.; Eric, M.G. Sol-gel derived V_2O_5-TiO_2 mesoporous materials as catalysts for the total oxidation of chlorobenzene. *Catal. Commun.* **2011**, *1*, 1–5.

18. Huang, H.; Gu, Y.; Wang, X. Catalytic combustion of chlorobenzene over VO_x/CeO_2 catalysts. *J. Catal.* **2015**, *326*, 54–68. [CrossRef]
19. Heo, U.S.; Kim, D.W.; Kim, K.S.; Park, D.W.; Heo, U.S. A facile synthesis of anatase TiO_2-Graphene nanocomposites using plasma and heat treatment. *Appl. Surf. Sci.* **2019**, *474*, 118–126. [CrossRef]
20. Zhao, K.; Han, W.; Tang, Z.; Lu, J.; Hu, X. High-Efficiency Environmental-Friendly Fe-W-Ti Catalyst for Selective Catalytic Reduction of NO with NH_3: The Structure-Activity Relationship. *Catal. Surv. Asia* **2018**, *22*, 20–30. [CrossRef]
21. Freidel, I.M.; Frost, A.C.; Herbert, K.J.; Meyer, F.J.; Summers, J.C. New catalyst technologies for the destruction of halogenated hydrocarbons and volatile organics. *Catal. Today* **1993**, *17*, 367–382. [CrossRef]
22. Hou, X.; Wang, Y.; Yang, Y.; Hu, R.; Yang, G.; Feng, L.; Suo, G. Microstructure evolution and controlled hydrolytic hydrogen generation strategy of Mg-rich Mg-Ni-La ternary alloys. *Energy* **2019**, *188*, 116081–116091. [CrossRef]
23. Zuo, S.; Ding, M.; Tong, J.; Feng, L.; Qi, C. Study on the preparation and characterization of a titanium-pillared clay-supported CrCe catalyst and its application to the degradation of a low concentration of chlorobenzene. *Appl. Clay Sci.* **2015**, *105*, 118–123. [CrossRef]
24. Kan, J.; Deng, L.; Li, B.; Huang, Q.; Zhu, S.; Shen, S.; Chen, Y. Performance of Co-doped Mn-Ce catalysts supported on cordierite for low concentration chlorobenzene oxidation. *Appl. Catal. A Gen.* **2017**, *530*, 21–29. [CrossRef]
25. Dai, Q.; Bai, S.; Wang, J.; Li, M.; Wang, X.; Lu, G. The effect of TiO_2 doping on catalytic performances of Ru/CeO_2 catalysts during catalytic combustion of chlorobenzene. *Appl. Catal. B Environ.* **2013**, *142*, 222–233. [CrossRef]
26. Hou, X.; Wang, Y.; Hu, R.; Shi, H.; Feng, L.; Suo, G. Catalytic effect of EG and MoS_2 on hydrolysis hydrogen generation behavior of high-energy ball-milled Mg-10wt.%Ni alloys in NaCl solution-A powerful strategy for superior hydrogen generation performance. *Int. J. Energy Res.* **2019**, *43*, 8426–8438.
27. He, C.; Yu, Y.; Shen, Q.; Chen, J.; Qiao, N. Catalytic behavior and synergistic effect of nanostructured mesoporous $CuO\text{-}MnO_x\text{-}CeO_2$ catalysts for chlorobenzene destruction. *Appl. Surf. Sci.* **2014**, *297*, 59–69. [CrossRef]
28. Dai, Y.; Wang, X.; Li, D.; Dai, Q. Catalytic combustion of chlorobenzene over Mn-Ce-La-O mixed oxide catalysts. *J. Hazard. Mater.* **2011**, *188*, 132–139.
29. Wang, X.; Kang, Q.; Li, D. Low-temperature catalytic combustion of chlorobenzene over $MnO_x\text{-}CeO_2$ mixed oxide catalysts. *Catal. Commun.* **2008**, *9*, 2158–2162. [CrossRef]
30. Murillo, R.; García, T.; Aylón, E.; Callén, M.S.; Navarro, M.V.; López, J.M.; Mastral, A.M. Adsorption of phenanthrene on activated carbons: Breakthrough curve modeling. *Carbon* **2004**, *42*, 2009–2017. [CrossRef]
31. Mastral, A.M.; García, T.; Callén, M.S.; Navarro, M.V. Assessement of Phenanthrene Removal from Hot Gas by Porous Carbons. *Energy Fuel* **2000**, *15*, 1–7. [CrossRef]
32. Nuño, M.; Adamaki, V.; Tobaldi, D.M.; Hortigüela-Gallo, M.J.; Otero-Irurueta, G.; Bowen, C.R.; Ball, R.J. Solid-Gas Phase Photo-Catalytic Behaviour of Rutile and TiO_n (1 <n <2) Sub-Oxide Phases for Self-Cleaning Applications. *Materials* **2019**, *12*, 170.
33. Zhang, H.; Xu, Y.; Liu, X. Study on preparation mechanism of $Ce\text{-}Cu/TiO_2$ hollow microspheres with uniform particle size distribution based on fourier transform infrared spectrum and X-ray diffraction. *Spectrosc. Spectr. Anal.* **2019**, *39*, 2360–2365.
34. He, H.; Dai, H.X.; Au, C.T. Defective structure, oxygen mobility, oxygen storage capacity, and redox properties of RE-based (RE = Ce, Pr) solid solutions. *Catal. Today* **2004**, *90*, 245–254. [CrossRef]
35. Hou, X.; Wang, L.; Yang, Y. Enhanced hydrogen generation behaviors and hydrolysis thermodynamics of as-cast Mg-Ni-Ce magnesium-rich alloys in simulate seawater. *Int. J. Hydrogen Energy* **2019**, *44*, 24086–24097. [CrossRef]
36. Harish, S.; Sabarinathan, M.; Archana, J.; Navaneethan, M. Functional properties and enhanced visible light photocatalytic performance of V 3 O 4, nanostructures decorated ZnO nanorods. *Appl. Surf. Sci.* **2017**, *418*, 171–178. [CrossRef]
37. Dong, G.; Bai, Y.; Zhang, Y.; Zhao, Y. Effect of the V4+(3+) V5+ ratio on the denitration activity for $V_2O_5\text{-}WO_3TiO_2$ catalysts. *N. J. Chem.* **2015**, *39*, 3588–3596. [CrossRef]

38. Ganduglia-pirovano, M.V.; Popa, C.; Sauer, J.; Abbott, H.; Uhl, A.; Baron, M.; Stacchiola, D.; Bondarchuk, O.; Shaikhutdinov, S.; Freund, H.J. Role of Ceria in Oxidative Dehydrogenation on Supported Vanadia Catalysts. *J. Am. Chem. Soc.* **2010**, *132*, 2345–2349. [CrossRef]
39. Zhang, H.; Fangm, Y. Temperature dependent photoluminescence of surfactant assisted electrochemically synthesized ZnSe nanostructures. *J. Alloys Compd.* **2019**, *781*, 201–208. [CrossRef]
40. Dandekar, A.; Baker, R.T.K.; Vannice, M.A. Characterization of activated carbon, graphitized carbon fibers and synthetic diamond powder using TPD and DRIFTS. *Carbon* **1998**, *36*, 1821–1831. [CrossRef]
41. Shangguan, J.; Li, C.; Miao, M.; Yang, Z. Surface characterization and SO_2 removal activity of activated semi-coke with heat treatment. *N. Carbon Mater.* **2008**, *23*, 37–43. [CrossRef]
42. Biniak, S.; Szymański, G.; Siedlewski, J.; Swiatkowski, A. The characterization of activated carbons with oxygen and nitrogen surface groups. *Carbon* **1997**, *35*, 1799–1810. [CrossRef]
43. Poelman, H.; Sels, B.F.; Olea, M.; Eufinger, K.; Paul, J.S.; Sack, I. New supported vanadia catalysts for oxidation reactions prepared by sputter deposition. *J. Catal.* **2007**, *245*, 156–172. [CrossRef]
44. Arena, F.; Trunfio, G.; Negro, J.; Spadaro, L. Optimization of the $MnCeO_x$ system for the catalytic wet oxidation of phenol with oxygen (CWAO). *Appl. Catal. B Environ.* **2008**, *85*, 40–47. [CrossRef]
45. Arena, F.; Trunfio, G.; Negro, J.; Fazio, B.; Spadaro, L. Basic Evidence of the Molecular Dispersion of $MnCeO_x$ Catalysts Synthesized via a Novel "Redox-Precipitation" Route. *Chem. Mater.* **2007**, *38*, 2269–2276. [CrossRef]
46. Nagano, S.; Tamon, H.; Adzumi, T.; Nakagawa, K.; Suzuki, T. Activated carbon from municipal waste. *Carbon* **2000**, *38*, 915–920. [CrossRef]
47. Zhou, X.J.; Buekens, A.; Li, X.D.; Chen, K.F. Adsorption of polychlorinated dibenzo-p-dioxins/dibenzofurans on activated carbon from hexane. *Chemosphere* **2016**, *144*, 1264–1269. [CrossRef]
48. Wang, J.; Chen, Z.; Chen, B. Adsorption of polycyclic aromatic hydrocarbons by graphene and graphene oxide nanosheets. *Environ. Sci. Technol.* **2014**, *48*, 4817–4825. [CrossRef]

© 2019 by the authors. Licensee MDPI, Basel, Switzerland. This article is an open access article distributed under the terms and conditions of the Creative Commons Attribution (CC BY) license (http://creativecommons.org/licenses/by/4.0/).